Int. J. Electrochem. Sci., 17 **(2022)** Article Number: 220231, doi: 10.20964/2022.02.41

International Journal of
ELECTROCHEMICAL
SCIENCE
www.electrochemsci.org

Short Communication

Design and Study of Ta/P co-doped $SrFeO_{3-\delta}$ as Cathode for Solid Oxide Fuel Cells

Dongliang Dai[*], *Yang Liu, Hao Qiu, Dongpo Xiao, Hao Jiang*

School of Energy and Power Engineering, Jiangsu University of Science and Technology, Zhenjiang, 212003, China.
[*]E-mail: dldaijust@163.com

Received: 6 November 2021 / *Accepted:* 13 December 2021 / *Published:* 5 January 2022

As a new type of energy conversion device with high efficiency and environmental protection, SOFC (Solid Oxide Fuel Cell) is a very attractive energy conversion device. However, the most important factor limiting the development of SOFC is its high operating temperature, which affects its commercial development. Therefore, optimizing the internal structure of the electrode and developing low temperature cathode materials are also important directions for the future development of solid oxide fuel cells. Due to the different metal and nonmetal doping will have different effects on the performance of SOFC. In this experiment, we have synthesized the Ta/P co-doped $SrFeO_{3-\delta}$ based cathode material $Sr(Fe_{0.9}Ta_{0.1})_{0.95}P_{0.05}O_{3-\delta}$(STFP) by solid phase method. The feasibility of the cathode material was verified by XRD imaging analysis, oxygen non-stoichiometric ratio analysis, conductivity test, symmetrical cell impedance test, single cell output power test and SEM electron microscope analysis. According to the conductivity test, the maximum of STFP at 690 ℃ is 43.3 S cm^{-1}. Symmetrical cells were sintered at 1000 ℃, 900 ℃ and 800 ℃ respectively, the area specific resistance (ASR) results showed that the best sintered performance is at 800 ℃ and the minimum ASR at 750 ℃ is 0.092 Ω cm^2 for STFP cathode based on $Sm_{0.2}Ce_{0.8}O_{1.9}$ (SDC) electrolyte. Meanwhile, at 700 ℃ the maximum power density of single cell sintered at 800℃ is 694 mW cm^{-2}.The results show that STFP can be used as a candidate cathode material.

Keyword: solid oxide fuel cell; co-doped; strontium ferrite cathode.

1. INTRODUCTION

Energy is the basis for human development and with the improvement of living standard, the demand for energy is increasingly urgent. However, the over-exploitation of fossil energy by human beings leads to the increasing shortage of fossil energy storage on earth. The inefficient use of fossil energy not only wastes a lot of energy resources, but also causes environmental pollution and ecological deterioration. Therefore, the development of new energy and advanced energy conversion

technology is of vital importance to today's society [1-4]. In the past decade, more and more attention has been paid to the research and development of fuel cell technology [5,6]. Solid oxide fuel cell (SOFC) is considered one of the most promising fuel cell technologies for its high efficiency, low pollution and ability to convert the chemical energy of the fuel directly into electricity. However, because of the high operating temperature of SOFC, it can not be used in wide range of applications, which greatly limits its commercial development. Therefore, how to reduce the operating temperature of SOFC while maintaining excellent performance is the direction of research [7]. We know that low operating temperatures causes SOFC output performance to degrade rapidly [8]. Therefore, our goal is to develop cathode materials with excellent electrochemical catalytic properties at interintermedium and low temperatures.

In recent times, more and more excellent cathode materials have been developed. Typical cathode material $La_{0.8}Sr_{0.2}MnO_3$ (LSM) has good performance at high temperature, but its development is limited by poor Oxygen Reduction Reaction (ORR) activity at intermedium and low temperatures [9, 10]. Later, researchers studied Co and Fe based perovskite materials, which mainly include $BaCoO_{3-\delta}$ (BC) based, $SrCoO_{3-\delta}$ (SC) based and $SrFeO_{3-\delta}$ (SF) based perovskite cathode materials [11-14]. For single-phase perovskite, doping ions can improve the electrochemical activity of the cathode and the performance of the cathode . With the unremitting efforts of researchers, some cation-doped Co-based perovskite materials have been proved to be cathode electrode materials. For example, $La_{0.6}Sr_{0.4}Co_{0.2}Fe_{0.8}O_{3-\delta}$ (LSCF) [15], $Ba_{0.5}Sr_{0.5}Co_{0.8}Fe_{0.2}O_{3-\delta}$ (BSCF) [16], $Sm_{0.5}Sr_{0.5}CoO_{3-\delta}$ (SSC) [17] and $PrBaCo_2O_{5+\delta}$ [18], these materials have excellent ORR activity at low and intermedium temperatures. More and more $SrFeO_3$ based materials have been developed as cathodes. For example, Jiang developed Nb^{5+}doped SF perovskite $SrFe_{1-x}Nb_xO_{3-\delta}$, and a single cell based on Nb-doped SF cathode achieved a power output of 1403 mW cm^{-2} at 800 ℃ [19]. It has also been reported that $SrFe_{0.8}Nb_{0.2}O_{3-\delta}$ [20], $SrFe_{0.95}Ti_{0.05}O_{3-\delta}$ [21], $SrFe_{0.9}Ti_{0.1}O_{3-\delta}$ [22] and other materials can also be used as cathode materials, and show good cathode performance through doping B-site ion. Herein, we synthesized P and Ta co-doped $SrFeO_{3-\delta}$ material, and verified it as a potential cathode material through various characterization and cell performance analysis.

2. EXPERIMENTAL

2.1 Synthesis and fabrication

$Sr(Fe_{0.9}Ta_{0.1})_{0.95}P_{0.05}O_{3-\delta}$(STFP) powder was synthesized by solid phase method. By mixing stoichiometric $SrCO_3$, Fe_2O_3, Ta_2O_5, H_6NO_4P into a planetary ball mill with rotational speed of 400 rpm for 24 h. The powder was dried and ground into powder, then pressed it into pellets and sintered it at 800 °C for 10 h. Next, the sintered pellets were re-ground and pressed into pellets in the same way. Finally, sintered the pellets at 1200 °C for 10 h and we can obtain the STFP powder after grounding. Afterwards, we used the obtained STFP powders for XRD tests. Weighed the STFP powder and grind it well with polyvinyl butyral (PVB), then pressed into dimensional strips by dry pressing method, calcined it in a muffle furnace at 1200 °C for 10h to obtain the test sample, which was then used for conductivity testing.

An iodometric titration method was used to determine the average valence of the B-site variable metal cations in the STFP cathode material and then calculated the non-chemometric value of oxygen (δ) according to the principle of electrical neutrality. The iodometric titration was carried out as follows: the STFP powder is completely dissolved with hydrochloric acid in a volume ratio of 1:1 (HCL:H_2O), followed by the addition of KI, which is diluted with an appropriate amount of deionised water. Water-soluble starch was then added dropwise to obtain a dark blue solution, after which a titration was carried out using 0.01944 mol L^{-1} of $Na_2S_2O_3$ until the solution changed to a light pink colour (the end point of the titration) and the volume of $Na_2S_2O_3$ consumed was recorded. Finally the oxygen non stoichiometric ratio (δ) is calculated from the chemical equation.

SDC powder were synthesis EDTA–citric acid as reported [23]. The synthesized SDC powder was pressed into disk shape pellets, and then calcined at 1400℃ for 5h to form a dense structure of the electrolyte. Then, the prepared cathode slurry was sprayed onto both sides of SDC electrolyte pellet and calcined it at 1000 ℃, 900 ℃ and 800 ℃ for 2h in air to form symmetrical cells for electrochemical impedance spectroscope (EIS). To measure the cell output performance, we made a single cell with the structure of STFP|SDC| NiO-SDC. Firstly, NiO-SDC (70:30 wt%) anode powder was pressed with SDC powder to get NiO-SDC|SDC double-layer bilayer billet. Secondly, it was calcined at 1400 °C for 5h. Finally, STFP cathode slurry was sprayed onto the one side of the NiO-SDC|SDC double-layer bilayer billet and then calcined at 800 °C for 2h to form the single cells.

2.2. Characterization

In this experiment, a Bruker D8 advanced X-ray diffractometer was used to characterise the crystal structure of the synthesised STFP cathode material. The instrument uses a Cu-targeted Kα-ray source with a wavelength of 1.54056 Å and a continuous scan range of $10° \leq 2\theta \leq 90°$ with a scan step of 0.02°. The microstructure of single cell is through a fileld emission scanning electron microscope (FE-SEM, JEOL-S4800). To measure conductivity of STFP, it needs to adhere two silver wires on both sides of the sample with silver paste for conduction as voltage electrode, connect two silver wires between both sides as current electrode, and test the conductivity of cathode material by DC four probe method[24].

Electrochemical impedance spectroscope (EIS) is an electrochemical measurement using a small amplitude sine wave potential or current as the perturbation signal. EIS testing with Princeton Applied Research, the frequency range of it is 1 MHz ~ 0.1 Hz with an AC voltage of 10 mV. After that fitted using VersaStudio software, the EIS data were analysed using the relaxation time distribution method (DRT). In the single cell test, the manufactured cell is sealed with silver paste on a quartz tube. H_2 (80 mL/min) or a CH_4-O_2 gas mixture (CH_4: 100 mL/min, O_2: 50 mL/min) is injected into the anode side while the cathode side is exposed to ambient air using a Keithley 2440 sourcemeter to assess cell performance.

3. RESULTS AND DISCUSSION

3.1 Phase analysis

The principle of X-ray diffraction is that chalcogenide structure of the powder is irradiated by X-rays, different atoms scatter the X-rays and interfere, with different light intensities appearing in different directions [25-27]. As the microstructure of different materials varies, their X-ray diffraction patterns also vary, so the main method to study the phase-forming structure of materials is using X-ray diffraction. In this experiment, the STFP cathode powder sintered at 1200 °C for 10h in air was characterised by X-ray diffractometry and the results of which are shown in Figure. 1. By observation and analysis, the pattern is clear in phase without spurious peaks, and seven characteristic peaks appear at 32°, 41°, 47°, 58°, 68°, 77° and 86° respectively, indicating that the target product obtained is a single phase material and exhibits a cubic calcium titanate structure. Therefore, the cathode powder synthesized by the solid phase method at 1200 °C is well phased. The synthesized powder can be further investigated and more experiments can be conducted to demonstrate the feasibility of the STFP material as cathode for solid oxide fuel cells.

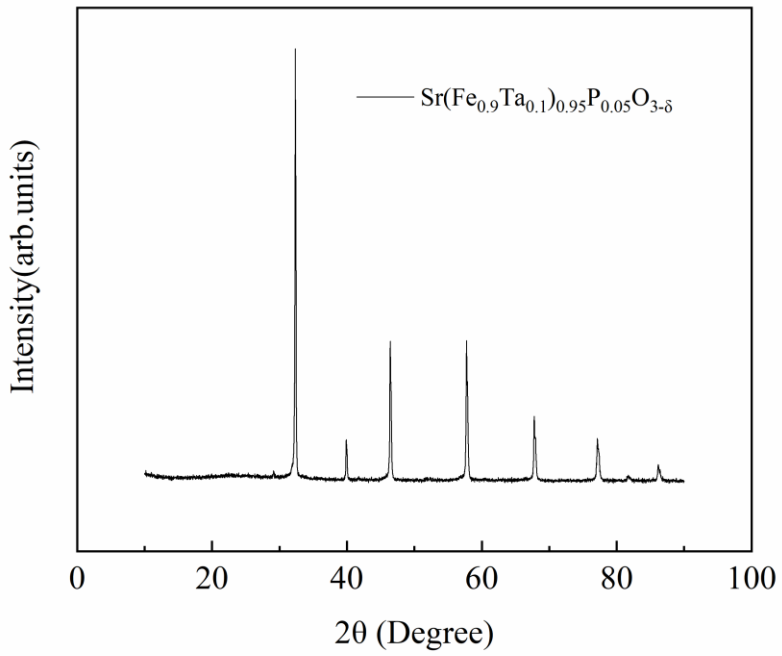

Figure 1. XRD patterns of SFTP cathode sintered at 1200 °C for 10h

3.2 Analysis of non stoichiometric titration results of oxygen

Redox titration is an analytical method based on the electron transfer, which is between the oxidizing and reducing agents in solution. $Na_2S_2O_3$ solution with a concentration of 0.01944moL L^{-1} was used as titrant and soluble starch solution as indicator for the titration of the synthesized powder in using the iodometric method. For single chalcogenide complex oxides, X_A denotes the average valence state at the A-position. The iodometric method allows the determination of the B-site cationic parity

state of the chalcogenide oxides as well as the non-chemical stoichiometry of the oxygen, based on the fact that the iodide ion reduces the higher valence metal ions such as Fe^{3+} and Fe^{4+} to their corresponding divalent ions, while I^- is reduced to I_2, the relevant chemical reaction equations are as follows:

$$B^{(2+x)+} + xI^- = B^{2+} + \frac{x}{2} I_2 \quad (1)$$

$$I_2 + 2S_2O_3^{2-} = 2I^- + S_4O_6^{2-} \quad (2)$$

Calculate the average valence (XB) of the metal ion at the B site and the oxygen non stoichiometric ratio (δ) in the sample from the following chemical equation[30-32]:

$$X_B = 2 + \frac{y}{k} = 2 + \frac{C \times V}{m/M} \quad (3)$$

$$\delta = 3 - \frac{X_A + X_B}{2} \quad (4)$$

Where C is the concentration of $Na_2S_2O_3$ (mol L^{-1}), V is the volume of $Na_2S_2O_3$ consumed by the titration (L), m is the mass of the powder (g), M is the molar mass of the oxide and X_A is the average valence of the A-site.

The calculation results are shown in Table 1:

Table 1. Calculation results of titration of the synthesized powder by iodimetry method

m (g)	M (g $molL^{-1}$)	V($Na_2S_2O_3$) L	C($Na_2S_2O_3$) mol L^{-1}	δ	M' (g $molL^{-1}$)	X_B
0.1091	196.587	0.037	0.019	0.345	196.587	3.310
0.1026	196.659	0.035	0.019	0.341	196.659	3.319
0.1042	196.287	0.035	0.019	0.364	196.287	3.273
Average	196.511			0.350	196.511	3.301

From Table 1, we can conclude that the three sets of δ values, by taking the average value we conclude that the final value of δ is 0.350.

3.3 Analysis of conductivity test results

The temperature dependence of electrical conductivities for STFP cathode material range from 300 °C～900 °C is showed in Figure. 2. Electrical conductivities result shows the same variation relationship with temperature in the temperature range of 300 °C～690 °C, which can be explained that STFP materials are semiconductor-like behavior in this range [28-30]. Furthermore, it reaches a maximum value of 43.3 S cm^{-1} at approximately 690 °C. Then, in the temperature range 690 °C～900 °C, the conductivities decrease with the rising of temperature, indicating the STFP material in this temperature range presents metal-like behavior.

Why the conductives of STFP change from semiconductor-like behavior to metal-like behavior, we can analyze it in two ways. In the front part, with the temperature increases, the carrier concentration in the material increases and the migration rate accelerates, it enhances the electrical

conductivity of the material [31]. So the electrical conductivity reaches maximum when the temperature rises to 690 °C. In the back part, with the further increases in temperature cause the lattice oxygen in the material to decompose, generating a large number of oxygen vacancies and electrons. At the same time, the high-valence Fe^{4+} is reduced to Fe^{3+}, leading to a reduction in the number of carriers and thus making the material less conductive. Hence, the Ta/P co-doped $SrFeO_{3-\delta}$ based cathode material STFP can meet the application of SOFC cathode materials.

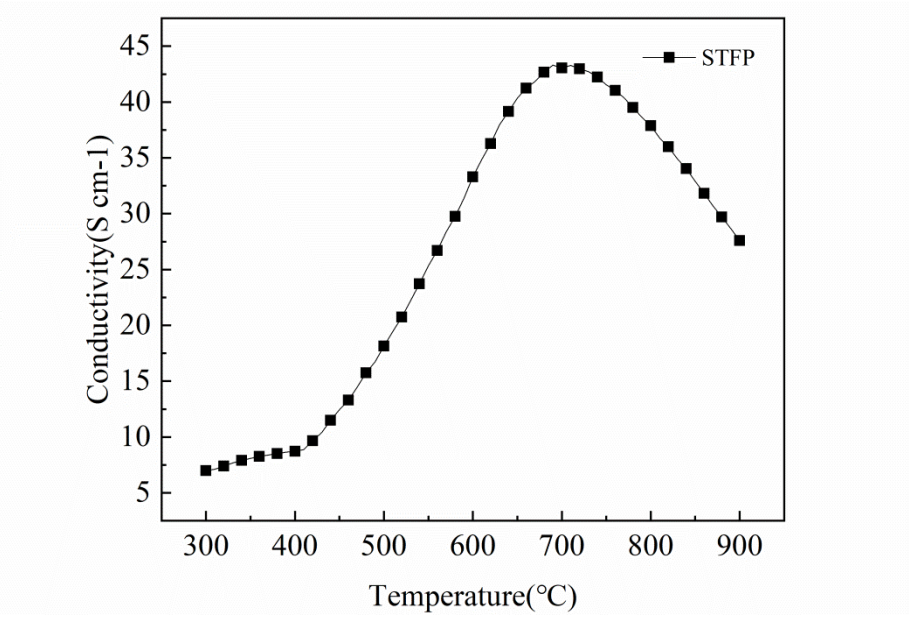

Figure 2. Electrical conductivity of STFP as a temperature range of 300 °C～900 °C

3.4 Analysis of electrochemical impedance spectroscopy

To investigate the oxygen reduction reaction (ORR) [32-34]characteristics of STPF, we sintered the symmetric cells at 1000 °C, 900 °C and 800 °C for 2h and tested them using ac impeance spectroscopy.

Table 2. Relationship between area specific resistance and temperature

Test temperature(℃)	R_P (Ω cm^2)		
	800 ℃	900 ℃	1000 ℃
750	0.092	0.159	0.150
700	0.186	0.292	0.273
650	0.408	0.570	0.555
600	1.009	1.412	1.255
550	2.741	3.675	2.972
500	9.348	10.970	9.372

Table 2 shows the variation of the area specific resistance (ASR) versus temperature for different STFP sintering temperatures. From the table, it can be seen that the symmetric cells sintered

at 800 °C exhibits the best electrochemical performance with the lowest value of ASR of 0.092 Ω cm^2 at 750 °C and indicates that the material has the best ORR activity when sintered it at 800 °C. Figures. 3(a) shows the EIS curves of the STFP cathode with SDC as the electrolyte at 800 °C for sintering temperatures in air. It can be seen from the Figures. 3(a), the impedance value of the cathodes all increase with the further temperature decreases, which is related to the fact that the electrode reaction at the cathode is a thermally excited process.

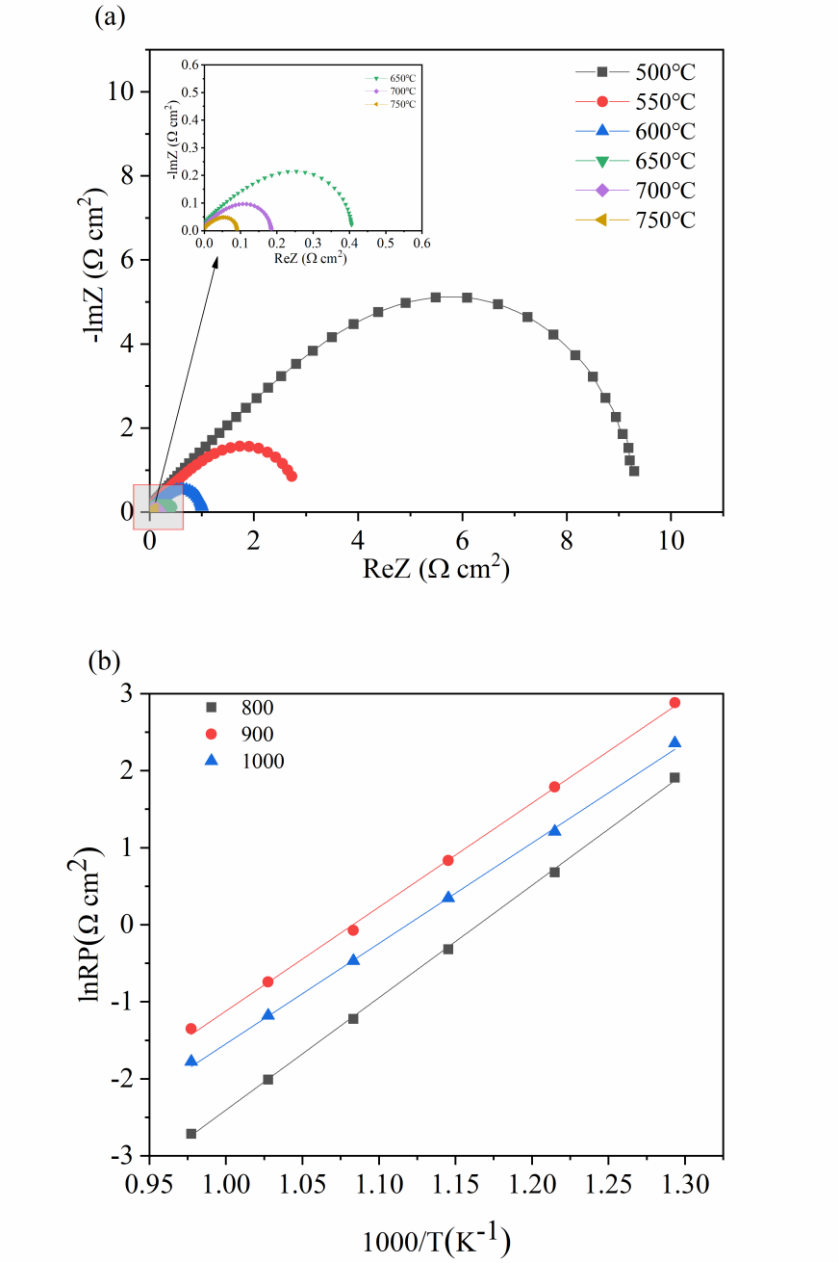

Figure 3. (a) The electrochemical impedance spectroscope curves of symmetric cells(STFP|SDC|STFP) with sintering temperatures of 800 ℃ in air; **(b)** Arrhenius diagram of symmetrical cells at different sintering temperatures

Activation energy can be used to indicate the minimum energy required for a chemical reaction to occur. Calculating the reaction activation energy of the symmetrical cell sintered at different temperatures was based on the measured data of symmetrical cell. Figure. 3(b) shows the arrhenius curves of the symmetric cell at different sintering temperatures and the reaction activation energy is obtained from the arrhenius equation. In Table 3, the reaction activation energy of the symmetrical cell sintered at 800 ℃ is 121 KJ mol^{-1} and the reaction activation energy of the symmetrical cell sintered at 900 ℃ is 112 KJ mol^{-1}.When the sintering temperature is 1000 ℃, the reaction activation energy of the symmetrical cell is 108 KJ mol^{-1}. In particular, the symmetrical cell sintered at 1000 ℃ has the smallest activation energy, indicating that the cell is more stable under the test conditions.

Table 3. Activation energy of battery reaction obtained at different sintering temperatures

Sintering temperature (℃)	Activation energy (Ea) $KJ \cdot mol^{-1}$
800℃	$121KJ \cdot mol^{-1}$
900℃	$112KJ \cdot mol^{-1}$
1000℃	$108KJ \cdot mol^{-1}$

In order to further investigate the individual processes of symmetric cells, a relaxation time distribution (DRT) analysis is required [35]. The relaxation time distribution method is a good response to the rate of change of perturbations caused by each reaction process and the analysis of each process can better optimise the performance of STFP materials, which can greatly reduce the unnecessary workload. Figure. 4 (a) shows the EIS（600 °C ~ 750 °C）of the DRT analysis of the symmetric cell at 800 °C sintering temperature. Each peak represents a particular reaction during the operation of an oxygen ion conductor type SOFC and the peak area reflects the polarisation value of each reaction. Relaxation time is the difference in time that required to restore equilibrium when thermal motion is disturbed, and it can also refer to the time which is required for the system to change from turbulent state to equilibrium state after disturbance caused by a variable in the system. The magnitude of the relaxation time is a good indication of how quickly the system recovers from equilibrium and a large relaxation time indicates a slower recovery. The peaks at the same temperature are represented by P1 to P5, P1 is the diffusion of oxygen ions into the electrolyte, P2 is the adsorption and dissociation of hydrogen in the anode, P3, and P4 are generally considered to be associated with cathodic reactions including: oxygen adsorption and dissociation on the cathodic surface oxygen reduction, oxygen diffusion to the boundary, and P5 being anodic gas diffusion.

Figure. 4 (b) shows the polarisation resistance as a percentage of each peak, with the P3, P4 peaks associated with the cathodic reaction dominating in the temperature range of 600 °C to 700 °C, indicating that the oxygen behaviour of the STPF cathode in terms of adsorption, dissociation, reduction and diffusion needs to be further optimised to further improve its ORR activity. At 750 °C, the P1, P2 peaks dominate, indicating better ORR activity at 750 °C, which validates the reason for the smallest ASR value at 750 °C. In summary, the results of the DRT analysis not only clearly

demonstrate the polarisation process of the cell, but also point the way to the further development of high-performance electrodes.

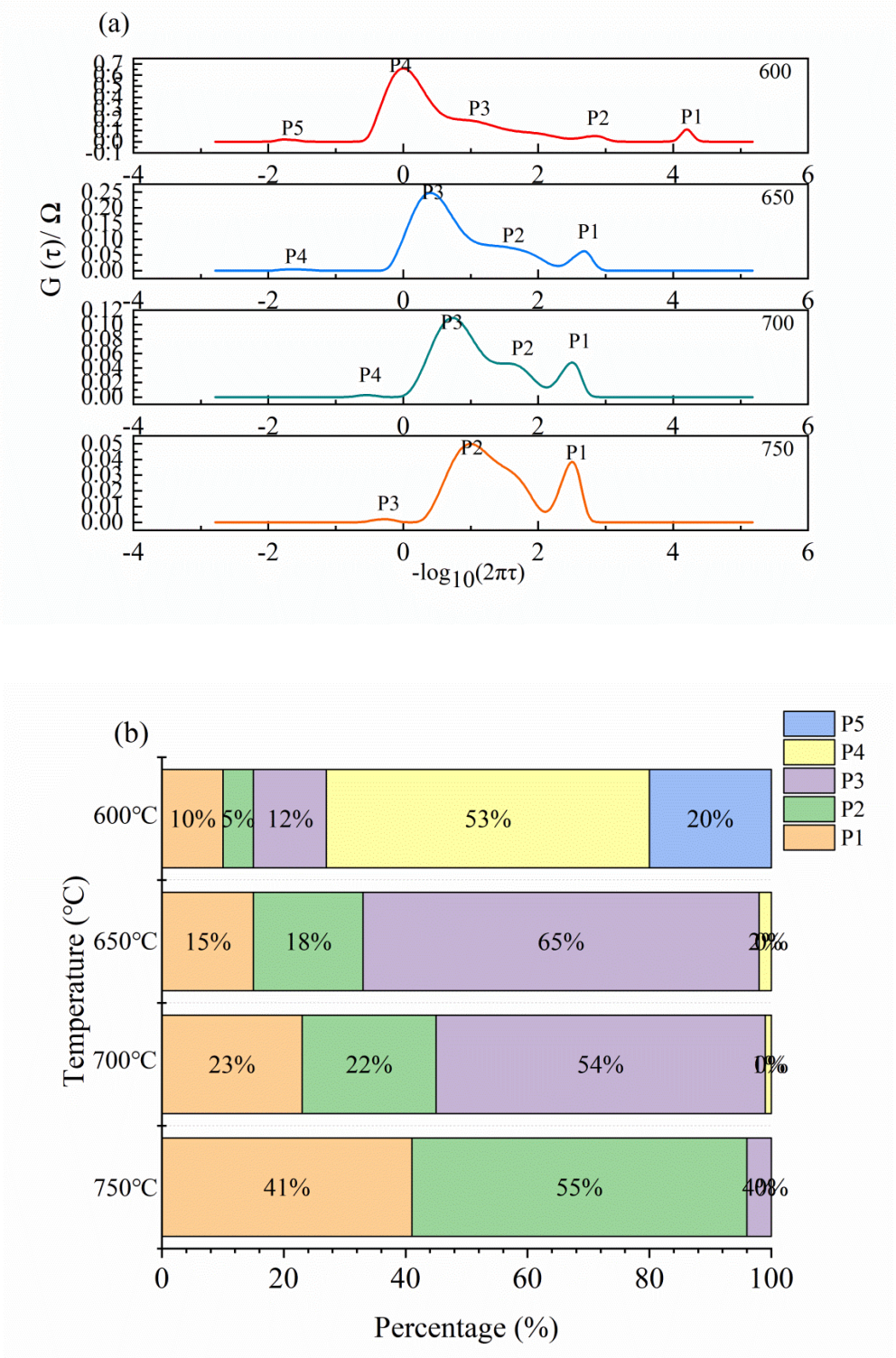

Figure 4. (a) DRT mapping of the symmetric cells EIS at 600 °C ~ 750 °C and **(b)** The ratio of the resistance value of each reaction step to the whole Rp value.

3.5 Single cell performance analysis

Table 4 shows the comparison of single cell performance of different doped $SrFeO_{3-\delta}$ materials as solid oxide fuel cell cathodes with hydrogen as fuel at 700°C. The single cell with STFP as cathode at 700 °C achieves a power density of 694 mW cm^{-2}. It can be seen from the table, the performance of Ta/P-doped cathode materials at the same temperature is higher than some reported $SrFeO_{3-\delta}$ chalcogenide cathode materials, such as $SrW_{0.2}Fe_{0.8}O_{3-\delta}$ (488 mW cm^{-2}) [37], $SrNb_{0.1}W_{0.1}Fe_{0.8}$ $O_{3-\delta}$(594 mW cm^{-2}) [38],$SrNb_{0.2}Fe_{0.8}$ $O_{3-\delta}$ (650 mW cm^{-2}) [19].

Table 4. Comparison of single-cell performance of co-doped $SrFeO_{3-\delta}$ as solid oxide fuel cell cathode

Ref	Cell type	Operation mode	Power density (mW cm^{-2})	T(°C)
This work	NiO-SDC|SDC|$Sr(Fe_{0.9}Ta_{0.1})_{0.95}P_{0.05}O_{3-\delta}$	H_2	694	700
[36]	NiO-YSZ|YSZ|CGO|$SrFe_{0.7}Cu_{0.3}O_{3-\delta}$	H_2	858	700
[37]	NiO-LSGM|LSGM|$SrW_{0.2}Fe_{0.8}O_{3-\delta}$	H_2	488	700
[38]	NiO-LSGM|LSGM|$SrNb_{0.1}W_{0.1}Fe_{0.8}O_{3-\delta}$	H_2	594	700
[19]	NiO-YSZ|YSZ|$SrNb_{0.2}Fe_{0.8}$ $O_{3-\delta}$	H_2	650	700

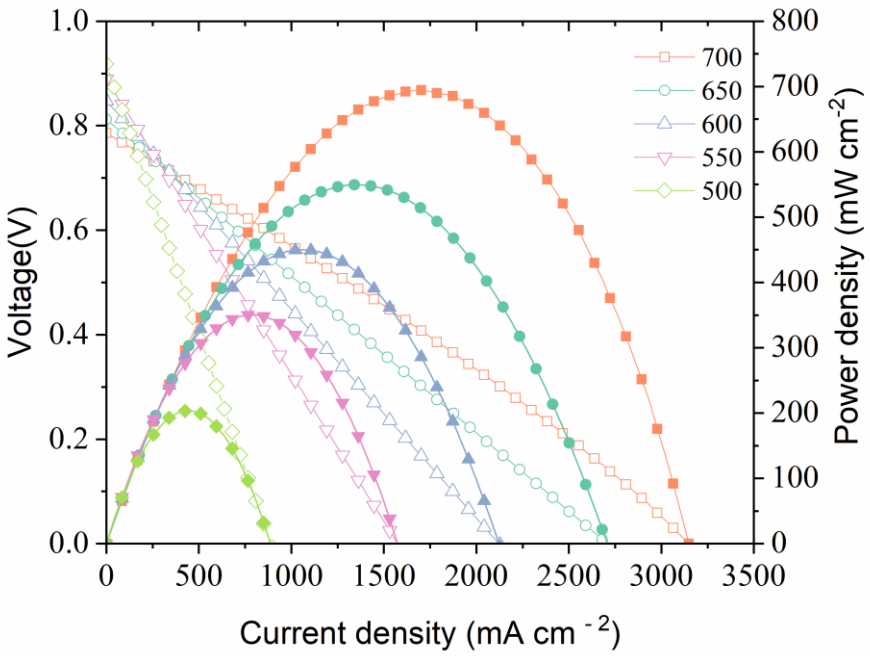

Figure 5. I–V and I-P curves of the cell with the configuration of STFP|SDC| NiO-SDC operating on hydrogen.

It can be seen from the Figure. 5 that the open circuit voltage (OCV) was 0.918 V ~ 0.786 V between 500 ~ 700 ℃ when the cell operated on hydrogen fuel and OCV decreased steadily with the temperature increased. Peak power densities (PPDs) were achieved at 203 mW cm^{-2}, 350 mW cm^{-2}, 450 mW cm^{-2}, 550 mW cm^{-2}, 694 mW cm^{-2} respectively at 500 °C, 550 °C, 600 °C, 650 °C, 700 °C. It can be seen from the graph that PPDs decreases with decreasing temperature, which is because the activation voltage is higher at lower temperatures, resulting in lower output voltage and lower power densities at the same current [39]. In addition, the power density of 694 mW cm^{-2} at 700 °C indicates a good performance of the cell.

3.6 Microstructure analysis

From the above analysis, we know that STFP can be used as the cathode materials of intermedium-low temperature solid oxide fuel cell and it shows good performance. We then further analyze the microstructure of the single cell composed of the material by electron microscopy to verify the stability of the single cell structure after operation. The Figure. 6 shows the section morphology of a single cell after testing. We can clearly find that the cathode and anode are relatively loose and porous, which can efficiently transmit gas. The electrolyte is completely sintered and dense, which can effectively isolate the gas diffusion between anode and cathode, ensuring the safe operation of the cell. The good contact between SDC electrolyte and adjacent materials is beneficial to reduce the interface electrochemical impedance and improve the cell performance. The results show that there is no delamination between electrolyte SDC and electrode material after cell operation and the electrode structure is relatively stable, which also indicates that STFP is a potential SOFC cathode candidate material.

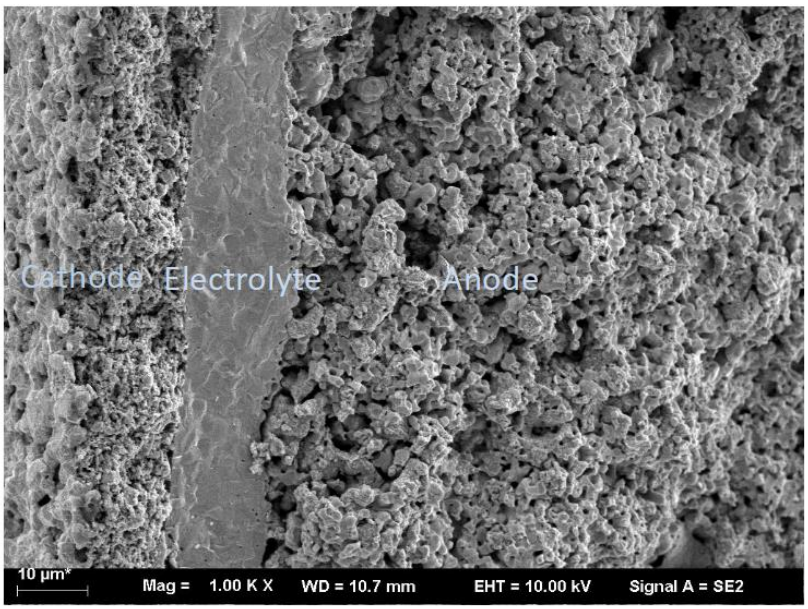

Figure 6. The section morphology of anode supported single cell after testing

4. CONCLUSION

We investigated the feasibility of P and Ta co-doped $Sr(Fe_{0.9}Ta_{0.1})_{0.95}P_{0.05}O_{3-\delta}$ materials as cathode materials for intermedium temperature SOFC. The following conclusions were drawn from the experimental verification: Firstly, the phase analysis indicates that STFP is a single-phase cubic chalcogenide structure. Secondly, from the conductivity test, we know that STFP has a maximum conductivity of 43.3 S cm^{-1} at 690 °C. Secondly, the STFP symmetric cell calcined at 800 °C, it has a minimum ASR of 0.092 Ω cm^2. Thirdly, the good ORR activity is due to the co-doping of P and Ta, which gives the good power density later, at 700 °C the maximum power density was achieved at 694 mW cm^{-2}. From the above experimental results and our analysis, we can know that STFP is a good cathode candidate material with excellent performance. Of course, we also look forward to the emergence of better and better cathode materials.

ACKNOWLEDGMENTS
We acknowledge the supports from Fuel Cell Preparation Laboratory, School of Energetics, Jiangsu University of Science and Technology.

References

1. L.P. Sun, N.L. Qiang, L.L. Huo, H. Zhao, *J. Alloys Compd.*, 12 (2021) 885.
2. Y. Chuangang, J.X. Yang, H.X. Zhang, *J. Alloys Compd.*, 234 (2021) 883.
3. P.J. Hoon, L.J. Ho, Y.K. Hoon, H. Kim, *Acta Mater.*,14 (2020) 206.
4. X. Wei, X.L. Liu, F.J. Jin, X.L. Jia, S.Yu, J.H. Li, *Electrochim. Acta*,76 (2020) 364.
5. S.S. Sapre, K. Pareek, R. Rohan. *Sci. Total Environ*, 24 (2021)11.
6. Q. Bing, Y.Y. Hu, C.Y. Tang, Y.C. Chen, J.H. Cheng, *Sci. Total Environ*., 45 (2021) 792.
7. G.D. Li, Y.J. Gou, J.S. Qiao, W. Sun, Z.H. Wang, K.N. Sun, *J. Power Sources*, 61 (2020) 477.
8. Z. Xing, C.P. Jiang, D. Tian, B.B. Admasu, *Mater. Lett.*, 78 (2021) 295.
9. B.M. Ricoult, K. Adib, T.S. Clair, *Solid State Ionics*, 179 (2008) 891.
10. J. Nielsen, M. Mogensen, *Solid State Ionics*, 189 (2011) 74.
11. S.E. Hou, J.A. Alonso, J.B. Goodenough, *J. Power Sources*, 195 (2010) 280.
12. F. Dong, Y. Chen, Z. Shao, *J. Mater. Chem. A*, 85 (2013) 9781.
13. D. Chen, C. Chen, F. Dong, *J. Power Sources*, 250 (2014) 188.
14. S. Molin, W. L. Iwaniak, P. Jasinski, *J. Electroceram.*, 28 (2012) 80.
15. A. Esquirol, J. Kilner, N. Brandon, *Solid State Ionics*, 175 (2004) 63.
16. L. Yan, M.Cheng, Y. Dong, *Appl. Catal., B*, 66 (2006) 64.
17. T. Xia, W. Rauch, F. Chen, *Solid State Ionics*, 149 (2002) 11.
18. W. Wang, T.S. Peh, S.H. Chan, *ECS Trans.*, 25 (2009) 2271.
19. S.S. Jiang, J. Sunarsob, W. Zhou, R. Ran, Z. P. Shao, *J. Power Sources*, 298 (2015) 209.
20. J. Yi, M. Schroeder, M. Martin, *Chem. Mater.*, 25 (2013) 815.
21. X. Yu, W. Long, F. Jin, *Electrochim. Acta*, 123 (2014) 426.
22. G. Yang, C. Su, Y. Chen, *J. Eur. Ceram. Soc.*, 35 (2015) 2531.
23. D.J. Chen, R. Ran, Z.P. Shao, *J. Power Sources*, 195 (2010) 4661.
24. J. Kanghee, H. Jooyeon, R. Jiseung, L. Eunkyung, L. Heesoo, *Appl. Sci.*, 11 (2021) 4963.
25. M. Nazan, A. Nasima, F. Naila, D.B. Daniel, S.B. Reddy,H. Peter, *Mater. Chem. Phys.*, 34 (2021) 270.
26. H.Y. Q, T.H. Zhang, D. Liu, M.J. Cheng, B.F. Tu, *J. Power Sources*, 67 (2021) 506.

27. X.L. Liu, F.J. Jin, X.W. Liu, N. Sun, J.X. Li, Y. Shen, F. Wang, *Electrochim. Acta*, 98 (2021) 390.
28. C.G. Yao, J.X. Yang, H.X. Zhang, S. Chen, C. Kedi, *J. Alloys Compd*., 45 (2021) 883.
29. E. Squizzato, G. Carollo, A. Glisenti, *Int. J. Hydrogen Energy*, 46 (2021) 48.
30. Z. Wang, H.B. Sun, J. Li,Guo, X. Hu, *Int. J. Hydrogen Energy*, 48 (2021) 44.
31. S. Chen, J.C. Jin, H. Chen, L.C. Guo, *J. Alloys Compd.*, 110 (2021) 879.
32. E. Pikalova, N. Bogdanovich, A. Kolchugin, K.Shubin, L. Ermakova, N. Eremeev, A. Farlenkov, *Int. J. Hydrogen Energy*, 46 (2021) 32.
33. C. Madhuri, K. Venkataramana, J. Shanker, C. Vishnuvardhan , *J. Alloys Compd*., 123 (2020) 849.
34. J. Seungyeon, J. Hyeon, Y.H. Kim, N. Dragos, M.H. Jae, *Appl. Catal., B*, 86 (2020) 23.
35. J.Y. Chena, J. Lib, L.C. Jia, I. Moussac, B. Chia, J. Pua, *J. Power Sources* , 428 (2019) 13.
36. Q. Sun, L.P. Sun, Y.N. Dou, Q. Li, N. Li, H. Zhao, *J. Power Sources,* 497 (2021) 15.
37. C.G. Yao, H.X. Zhang, J.D. Yu, R.Y. Zhang, J. Meng, F.Z. Meng, *J. Alloys Compd.,* 797 (2019) 205.
38. C.G. Yao, H.X. Zhang,X.J. Liu, J.L. Meng, J. Meng, F.Z. Meng, *Ceram. Int*, 45 (2019) 7351.
39. H. Chen, T.L. Zhu, X.Y. Chen, Y.F. Bu, Q. Zhong, *J. Electrochem. Soc.*, 16 (2020) 167.